ACS OMEGA

http://pubs.acs.org/journal/acsodf

Article

Study on the Preparation of Clean Liquid Fuel by Wide Fraction High-Temperature Coal Tar Deep Hydro-Upgrading on a Pilot Plant Trickle Bed Reactor

Xiaoyong Fan,* Dong Li, Louwei Cui, Chunran Chang, Long Yan, and Bo Yang

Cite This: *ACS Omega* 2022, 7, 48163−48172

Read Online

ACCESS | Metrics & More | Article Recommendations

ABSTRACT: High-temperature coal tar contains a high content of heavy components, and the mechanism of its hydrogenation to fuel oil has not been completely revealed at present. In this work, clean environmental friendly fuel oil was obtained from wide fraction high-temperature coal tar (WHTCT) hydrotreated in a three-stage continuous pilot-scale trickle bed reactor filled with commercial catalysts. The effect of reaction temperature (345−405 °C), reaction pressure (10−18 MPa), and LHSV (0.2−0.4 h^{-1}) on the product properties was investigated while the hydrogen/oil ratio remained constant (2000:1). Simultaneously, four lumped kinetic models were established to study the effects of reaction conditions on each component and interconversion between them. The results showed that the increase in temperature and pressure and the decrease in LHSV can effectively improve the quality of products. Under the reaction conditions of a temperature of 390 °C, a pressure of 16 MPa, an LHSV of 0.25 h^{-1}, and a hydrogen/oil ratio of 2000:1, the S and N in the feedstocks can be reduced from 4600 and 6800 μg/g to 24.06 and 14.32 μg/g in the products, respectively. So WHTCT can be used as a suitable feed to obtain gasoline and low-freezing point diesel blending components through hydrogenation. Tail oil (TO) can easily be converted into diesel fraction (DF) and gasoline fraction (GF) with high selectivity. DF can be converted into GF only at higher temperatures, and GF hardly undergoes cracking to gas. The established kinetic model can accurately predict the content of TO, DF, GF, and gas of the products. Therefore, the results can provide a certain valuable reference for further development of industrial applications.

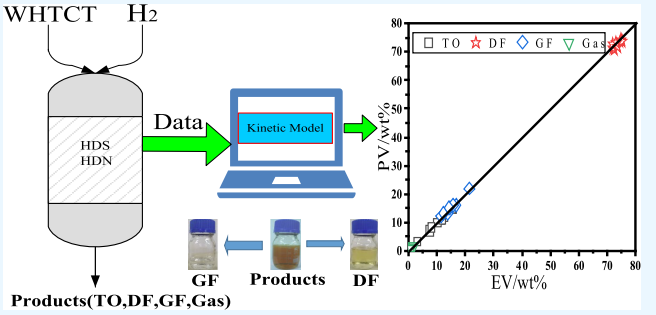

1. INTRODUCTION

With the reduction of global crude oil reserves, the exploration, development, and utilization of unconventional oils such as oil sands, oil shale, coal tar, and heavy oil are receiving unprecedented attention.[1] China is the world's largest coal producer. Coal is still China's main energy source. Coal tar obtained through the pyrolysis of coal has gradually become a supplementary raw material for the production of transportation fuels in refineries, which can be divided into two types according to different pyrolysis processes, including high-temperature coal tar (HTCT) and low-temperature coal tar (LTCT).[2] In recent years, China's coal tar output has basically stabilized at about 2200 × 10^4 t/a, of which LTCT can be a suitable raw material through hydrogenation to produce ultra-low heteroatom content traditional liquid fuels (such as gasoline and diesel), which has been paid much attention and obtained commercial application.[3,4] HTCT accounts for 80% of total coal tar production, produced by coal pyrolysis at a temperature of 900−1100 °C.[5] Compared with LTCT, HTCT possesses the characteristics of high density and viscosity with a high content of heavy components, making it more difficult to process.[6] Furthermore, influenced by traditional processing and utilization methods, HTCT hydrogenation to produce clean fuel technology develops slowly. Therefore, necessary consideration should be made to convert HTCT into light clean oil to improve its added value.[7]

In recent years, in the research of HTCT processing, various treatment processes based on supercritical fluid, suspended beds, and fixed beds have been reported in the literature. These processes generally involve reactions such as thermal cracking, catalytic cracking, and hydrocracking. Han et al.[7] studied the effect of supercritical water on the reaction of HTCT and showed that supercritical water can inhibit the coking and gas production and upgrade HTCT into light products and chemical products. Gu et al.[5] used supercritical gasoline as the

Received: September 26, 2022
Accepted: December 2, 2022
Published: December 15, 2022

Table 1. Main Properties of WHTCT

properties	unit	HTCT	WHTCT	properties	unit	HTCT	WHTCT
C	wt %	90.3	88.42	Ni	μg/g	0.42	0.26
H	wt %	5.12	8.23	V	μg/g	0.37	0.21
S	wt %	0.64	0.46	SARA analysis			
N	wt %	0.92	0.68	saturated hydrocarbon	wt %	0	0
O(diff.)	wt %	3.02	2.21	aromatic hydrocarbon	wt %	27.33	46.59
density (20 °C)	g/mL	1.174	1.09	resin	wt %	35.27	23.13
viscosity (50 °C)	mm^2/s	13.92	10.56	n-C_7asphaltenes	wt %	37.46	27.81
H/C atomic ratio		0.68	1.13	distillation range			
CCR	wt %	8.76	6.24	initial boiling point (IBP)	°C	171	129
ash	wt %	0.04	0.02	30%/50%	°C	318/405	260/319
Fe	μg/g	25.56	22.12	70%/90%	°C	497/565	360/455
Ca	μg/g	12.14	10.06	95%-final boiling point (FBP)	°C	584/−	496/508
Na	μg/g	9.78	8.32				

reaction solvent and Mo-Co-Pd-Y as the catalyst to study the hydrocracking behavior of HTCT and obtained a higher yield of light oil. Chang et al.[8] used Y zeolite catalysts in the hydrocracking of coal tar with supercritical gasoline and found that the catalyst has high hydrocracking activity and can effectively increase the yield of light oil. However, the supercritical process needs extremely harsh requirements for process equipment, greatly affecting its application in industry. Yuan and co-workers[1] carried out experimental research on HTCT hydrocracking in a suspended bed reactor and showed that the catalytic system can greatly reduce the yield of gas and coke and effectively increase the yield of total liquid.[9,10] Majka et al.[11] studied the hydrocracking performance of coal tar in the reactor and believed that the NiW/Al_2O_3 catalyst can promote the formation of light aromatics and the cracking activity of condensed aromatics.

The fixed-bed hydrogenation process is widely used in heavy oil processing and has certain advantages in the production of high-quality and environmentally friendly distillates.[12] HTCT contains 55−60% coal tar pitch, so that the hydro-upgrading of HTCT was usually carried out on the fixed-bed reactor by removing the pitch first. Zhao et al.[13] used combined hydrorefining-hydrocracking technology to hydro-upgrade anthracene oil and obtained distillate oil that can be used as a blending diesel component.However, only less than 30% of coal tar can be converted. Yan et al.[14] carried out a whole fraction HTCT hydrogenation test on a single-tube reactor, but still 20.27% of the tail oil could not be processed. In order to increase the yield of light distillate, different kinetic models have also been widely reported. Jarullah[15] proposed to establish a discrete lumped kinetic model to study the yield of each distillate fraction and believed that the amount of distillate oil could be increased under moderate operating conditions.

As previously articulated, HTCT has high density and viscosity, mainly composed of polycyclic aromatic hydrocarbon compounds with a large number of S, N, and O heteroatom compounds. Although there has been a lot of research on the lightening of HTCT, the research on its hydrogenation to produce clean fuel oil and the conversion law of each component [tail oil (TO), diesel fraction (DF), gasoline fraction (GF), and gas] in HTCT has not been widely reported. Therefore, the purpose of this work is to carry out a deep hydrogenation test for WHTCT in a three-stage continuous pilot-scale trickle bed reactor (TBR), to discuss the influence of process parameters on product performance, then to distill the product into DF, GF, and TO, and further to establish 4 lumped (TO, DF, GF, and gas) kinetic models according to the distillation range of the feedstock and products, studying the conversion law between the four components. It will provide a reference for hydrogenation of WHTCT to produce clean fuel oil in industy.

2. EXPERIMENTAL WORK

2.1. Feed Stock. A sample of HTCT from a coking plant in Shandong province was collected. After being dehydrated, the coal tar was distilled on a deep vacuum distillation unit, 60% of the total volume of the fraction was collected as the WHTCT, and the main properties are listed in Table 1. It can be seen that the density of the WHTCT is similar to that of heavy crude oil, but with lower the H/C atomic ratio (1.4∼1.7), no saturated hydrocarbon existed, and the content of conradson carbon residue (CCR) and ash is relatively close to that of the petroleum residue. WHTCT contains a high content of resin and asphaltene, mainly composed of polycyclic aromatic hydrocarbons with high aromaticity.

2.2. Catalyst Properties. WHTCT has a high asphaltene content. Therefore, the selected catalyst should have hydrorefining and hydrocracking function. Therefore, the Ni−Mo series of industrial catalysts were selected, in which Ni−Mo sulfides have good hydrogenation and hydrodesulfurization activities. The $SiO_2-Al_2O_3$ mixture contains Brönsted acid sites, which is beneficial to hydrocracking. The catalyst has also been proved to have excellent performance for heavy coal tar hydrogenation in the previous work.[16−18] The properties and composition of the catalyst are listed in Table 2.

2.3. Pilot Plant. The pilot-scale TBR reaction system consists of three fixed-bed reactors connected in series. As shown in Figure 1, the reaction system includes three parts: (1) Reactant feed system, which is composed of coal tar and high-pressure hydrogen supply pipelines. (2) Hydrogenation reaction system, which consists of three parallel (150 mL × 3) fixed-bed reactors, called R1, R2, and R3, respectively. The outer diameter of each reactor is 45 mm with an inner diameter of 29 mm, and the length of the static constant temperature zone is 300 mm. Each reactor is equipped with independent liquid and gas supply lines with product collection facilities wrapped in a heating shell. The heating shell is divided into three zones from top to bottom: preheating zone, catalyst heating zone, and post heating zone. R1 is filled with 270 mL of porcelain balls, 100 mL of catalyst, and 178 mL of porcelain balls, from top to bottom, while R2 and R3 are uniformly filled

https://doi.org/10.1021/acsomega.2c06202
ACS Omega 2022, 7, 48163−48172

Table 2. Properties and Compositions of Catalysts

type	HF
Main Chemical Components, wt %	
MoO_3	21.76
NiO	6.38
SiO_2	5.48
Na_2O	0.29
P_2O_5	4.27
Al_2O_3	balance
Main Physical Characteristics	
shape	trilobe
S_{BET}, $m^2\ g^{-1}$	217
pore volume, $cm^3\ g^{-1}$	0.45
bulk density, $cm^3\ g^{-1}$	0.75
pore diameter, nm	6.5
Mean Particle Diameter, mm	
mean particle length	1.8

with 220 mL of porcelain balls, 150 mL of catalyst, and 178 mL of porcelain ball from top to bottom. (3) Product separation and collection system, including a high-pressure separator and a product storage tank, which separates liquid from gas and collects liquid products. The preheated WHTCT and hydrogen flow co-currently down through the reactor and react. The whole test was carried out under the steady state.

2.4. Pilot Plant Test Procedure. A certain amount of fresh catalyst was crushed and sieved to the required average particle size (1.5−1.8 mm) and then loaded into the reactor. First, nitrogen gas (P > 16 MPa) was used to perform a leak test on the device, and then, it was switched to 16 MPa hydrogen for a leak test to ensure the safe operation of the device, reducing the hydrogen pressure to 8 MPa with a flow rate of 320 L/h. The reactor temperature was then heated to 170 °C (the heating rate was 10 °C/h). At 170 °C, the presulfided oil (composed of 2 vol % CS_2 and 98 vol % hydrogenated diesel) was pumped into the reactor at a rate of 400 mL/h. Then, the reactor temperature was increased to 230 °C and keep constant for 8 h, and then, the reactor temperature was increased to 260, 320, and 360 °C, and the operating conditions were fixed for 8 h. The H_2S concentration was checked to ensure that the catalyst completely presulfided.

According to the characteristics of the feedstock and the previous experience, this test is carried out at a reaction pressure of 12−18 MPa, a reaction temperature of 345−405 °C, an LHSV of 0.2−0.35 h^{-1}, and a constant H_2/oil ratio of 2000:1. Under each hydrogenation condition, the products were collected every 4 to 8 h after a stable period of 4 h, and then, the liquid products were distilled into GF (<180 °C), DF (180∼360 °C), and TO (>360 °C) for analysis.

2.5. Analysis Method of Feedstock and Products. The infrared absorption method after combustion in an induction furnace was used to determine the sulfur and nitrogen content in the product (TSN-2000SN, Jiangsu Jiangfen Instrument Co., Ltd.) according to SH 0689 and GB/T 17674. The distillation range was measured with an automatic distillation tester (Dalian Yuandongxing Instrument Co., Ltd.), and the implementation standard was GB/T 6536. The density was measured by a density meter (Anton Paar DMA 4100, Austria), and the viscosity was measured by a viscometer (HKYN-301, Wuhan Huadian Keyi Electric Co., Ltd.) according to GB/T 1884 and GB/T 265.The octane number (RON) of gasoline and the cetane number (CN) of diesel were tested with an octane number tester and a cetane number tester (RASX-100 M, Beijing Labtech Instruments Co., Ltd.) according to GB/T 5487 and GB/T 11139, respectively.

3. RESULTS AND DISCUSSION

3.1. Influence of Reaction Conditions on the Physical Properties of the Product. *3.1.1. Effect of Reaction Temperature.* Increasing the hydrogenation temperature can elevate the conversion rate, while the cracking and coking of the reactants will also increase, which will easily lead to catalyst deactivation. Therefore, an appropriate reaction temperature is needed for hydrogenation. Under five typical reaction temperatures of 345, 360, 375, 390, and 405 °C and other parameter conditions (P = 16 MPa, H_2/oil ratio = 2000:1, and LHSV = 0.25 h^{-1}), the effects of reaction temperature on product characteristics and component distribution were investigated, and the results are shown in Table 3.

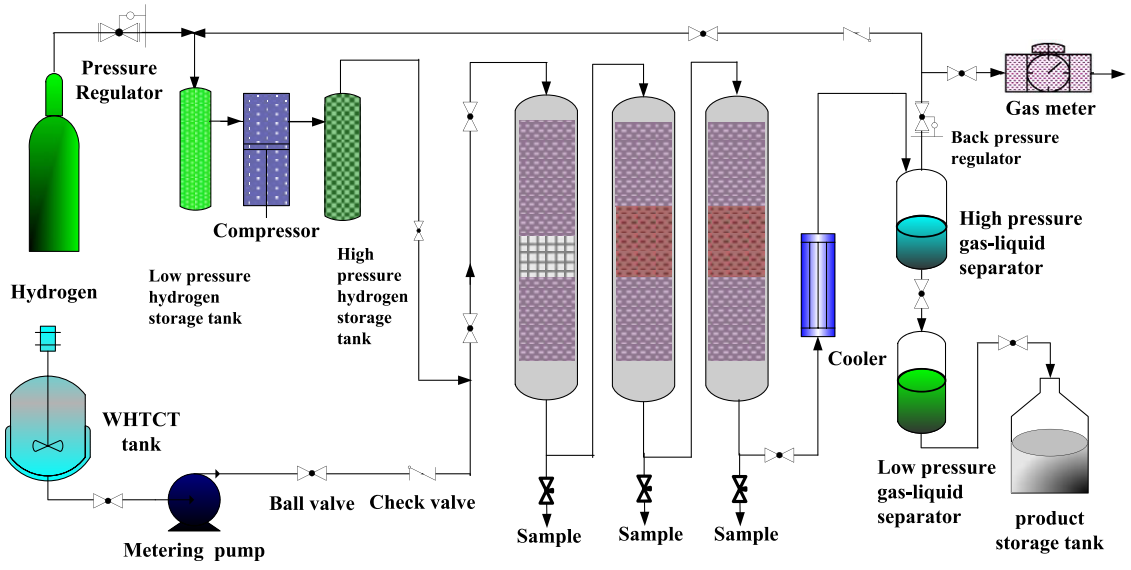

Figure 1. Hydrogenation process flow chart for WHTCT.

https://doi.org/10.1021/acsomega.2c06202
ACS Omega 2022, 7, 48163−48172

Table 3. Influence of Temperature on Product Characteristics and Component Distribution

	temperature/°C				
product characteristics	345	360	375	390	405
density (20 °C) (g mL^{-1})	0.92	0.9084	0.90	0.8996	0.8932
S ($\mu g\ g^{-1}$)	156.42	67.54	51.11	24.06	9.13
N ($\mu g\ g^{-1}$)	405.58	189.65	60.04	14.32	8.86
atomic H/C ratio	1.44	1.52	1.57	1.59	1.60
	Product Content (wt %)				
GF	10.03	12.66	14.14	16.71	21.56
DF	70.54	70.95	73.62	74.89	73.46
TO	19.21	15.85	11.42	7.45	3.14
gas	0.22	0.54	0.82	0.95	1.84

Table 4. Influence of Pressure on Product Characteristics and Component Distribution

	pressure/MPa				
product characteristics	10	12	14	16	18
density (20 °C) (g mL^{-1})	0.9280	0.9220	0.9150	0.8996	0.8982
S ($\mu g\ g^{-1}$)	154.04	105.58	37.32	24.06	23.35
N ($\mu g\ g^{-1}$)	195.82	111.73	74.04	14.32	11.24
atomic H/C ratio	1.35	1.38	1.46	1.59	1.61
	Product Content (wt %)				
GF	12.70	13.46	14.81	16.71	17.68
DF	70.56	73.65	74.68	74.89	75.06
TO	15.12	11.54	9.25	7.45	6.54
gas	1.62	1.35	1.26	0.95	0.72

The data in Table 3 show that increasing the temperature from 345 to 405 °C can effectively improve the H/C atomic ratio and reduce the sulfur and nitrogen content. The removal rate of S and N increases from 96.5 and 95.5% to 99.7 and 99.8%, respectively. The output of GF and DF also increased as well as gas ($C_1 \sim C_4$), indicating that a higher temperature is conducive to gas formation. The reduction of S and N at high temperatures can be attributed to several reasons: (1) A higher reaction temperature promotes intermolecular contact, which is beneficial to increase the chemical reaction rate and conducive to the reaction of refractory sulfur-containing and nitrogen-containing compounds with hydrogen.[19] (2) The increase in temperature and the decrease in viscosity accelerate the mass transfer rate between gas−liquid and solid−liquid, which is beneficial to increase the reaction rate of HDS and HDN.[20] (3) Increasing the temperature is conducive to the conversion of macromolecular compounds (gums and asphaltenes) in WHTCT into smaller molecules through mild hydrocracking. These small molecules more easily diffuse into the catalyst pores and reach the internal active sites to react. However, it has the highest HDN and HDS effects at 405 °C with the S and N content decreased from 4600 and 6800 $\mu g/g$ in the feedstock to 9.13 and 8.86 $\mu g/g$ in the products. However, when the temperature increases from 390 to 405 °C, the product properties have little change, but the gas content increases significantly, which greatly affects the yield of liquids. Futhermore, when the temperature is higher than 400 °C, the cracking and coking will increase, which will easily accelerate the catalyst deactivation.[21,22] Therefore, 390 °C can be selected as a more suitable reaction temperature.

3.1.2. Influence of Reaction Pressure. Pressure has a great influence on the hydrogenation process, and high pressures can effectively improve catalyst activity and increase the removal of impurities. However, considering safety and the costs of the hydrogenation unit, the lowest pressures were needed when obtaining the same product quality. Therefore, the conditions (T = 390 °C, LHSV = 0.25 h^{-1}, and H_2/oil ratio = 2000:1) remain unchanged, and the influence of reaction pressure (12∼18 MPa) on product performance is investigated. The results are listed in Table 4.

The data in Table 4 show that as the operating pressure increases, the reactivity of the reactants is enhanced, and the H/C atomic ratio of the product and the yield of GF and DF increase with the decreased density and S and N content. Due to the increase in pressure, the solubility of hydrogen in WHTCT increases, leading to diffusion from the liquid phase (oil) to the surface of the solid phase (catalyst) easily, which facilitates the contact between hydrogen, heteroatoms, and the catalyst and promotes the reaction.[16,23]

At a pressure of 14 MPa, 99% of sulfur-containing compounds can be removed, but with little change under a higher pressure. The nitrogen removal rate increased from 97.1% at 10 MPa to 99.8% at 18 MPa, indicating that the effect of pressure on HDN activity is greater than that of HDS within this pressure range. The reason is that, on the one hand, the increase in hydrogen pressure has a greater impact on the HDN reaction rate constant than on HDS; second, the removal of nitrogen requires hydrogenation saturation first, and a high pressure is beneficial to aromatic hydrogenation saturation. In addition, the removal rate of nitrogen is strongly dependent on the hydrogen pressure, and a high pressure is more beneficial to the HDN reaction,[24,25] which was also confirmed in this study. The increase in reaction pressure can effectively improve the quality of the product, but when the pressure is increased from 16 to 18 MPa, the content of S and N in the product remains almost unchanged, and the yield of GF and DF fluctuates within a narrow range. Based on safety and economic considerations, 16 MPa was selected as a more suitable reaction pressure.

https://doi.org/10.1021/acsomega.2c06202
ACS Omega 2022, 7, 48163−48172

Table 5. Influence of LHSV on Product Characteristics and Component Distribution

	LHSV/h^{-1}				
product properties	0.4	0.35	0.3	0.25	0.2
density (20 °C) (g mL^{-1})	0.9200	0.9084	0.9000	0.8996	0.8932
S ($\mu g\ g^{-1}$)	188.54	61.32	35.03	24.06	15.54
N ($\mu g\ g^{-1}$)	250.58	74.56	45.73	14.32	10.85
atomic H/C ratio	1.38	1.54	1.56	1.59	1.62
		Product Content (wt %)			
GF	10.2	12.43	14.69	16.71	19.91
DF	70.6	71.81	74.35	74.89	75.24
TO	18.78	15.22	10.23	7.45	3.32
gas	0.42	0.54	0.73	0.95	1.53

3.1.3. Influence of LHSV. LHSV was the ratio of the feed volume flow rate to the catalyst volume, which can reflect the interaction time between reactants and the catalyst. For the same catalyst bed, the smaller the LHSV value, the longer the contact time between the reactants and the catalyst. If the LHSV was determined, the catalyst loading amount can be predicted based on the conversion rate with the determined LHSV. Four typical LHSVs were chosen (0.2, 0.25, 0.3, 0.35, and 0.4 h^{-1}), and other parameters (P = 16 MPa, T = 390 °C, and H_2/oil = 2000:1) remain unchanged, and the impacts of LHSV on the characteristics and distribution of products are shown in Table 5.

As shown in Table 5, the LHSV decreased from 0.4 to 0.2 h^{-1}, the H/C atomic ratio of the product increased from 1.38 to 1.62, the sulfur and nitrogen content gradually decreased, the density decreased from 0.9200 to 0.8932 g/mL, the yield of GF and DF increased monotonously, and the TO content decreased from 18.78 to 3.32%. Because as the LHSV decreases, the contact time between the reactant molecules and the catalyst increases, which provides sufficient time for the reaction and can achieve higher conversion of heavy components.[21] WHTCT has a complex molecular composition, high content of heavy components, and high viscosity, resulting in a weak interaction between the gas phase (hydrogen), the liquid phase (coal tar), and the solid phase (catalyst). Therefore, WHTCT hydroprocessing should not be carried out under higher LHSV. When LHSV is reduced from 0.25 to 0.2 h^{-1}, little effect on HDS and HDN occurred. In addition, small LHSV can bring an increase in hydrogen consumption and a decrease in productivity. Therefore, 0.25 h^{-1} was a more suitable in this work.

The degree of HDS was higher than that of HDN at higher LHSV (>0.3 h^{-1}), which is consistent with a previous report.[26−28] It was mainly related to the different reaction mechanisms and reaction pathways for HDS and HDN. In the HDN process, the aromatic ring of the nitrogen-containing compound was saturated first, and then, the C−N bond was broken. However, the HDS reaction can be achieved by the direct hydrogenolysis of the C−S bond.[29,30]

When LHSV was lower than 0.25 h^{-1}, the HDN degree was slightly better than that of HDS, which means that the breaking rate of the C−N bond has increased. This was mainly because the lower LHSV can supply enough time for the refractory nitrogen-containing compound to adsorb on the weakly acidic catalyst, which makes the reaction of hydrogenation cleavage and the C−N bond saturation occur simultaneously,[31] resulting in a better HDN effect.

3.2. Oil Composition Analysis. The reaction lasts 600 h under the selected reaction conditions (P = 16 MPa, T = 390 °C, LHSV = 0.25 h^{-1}, and H_2/oil ratio = 2000:1), and about 30 L of liquid product was collected and then separated into GF, DF, and TO by an atmospheric distillation device. WHTCT and the separated sample were analyzed by Fourier transform infrared spectroscopy (FT-IR) analysis to reveal the functional group changes in the hydrogenation process, and gas chromatography−mass spectrometry (GC−MS) was used to analyze the chemical composition distribution of GF and DF.

3.2.1. FT-IR Analysis. The organic functional groups in WHTCT, products, GF, and DF are shown in Figure 2.

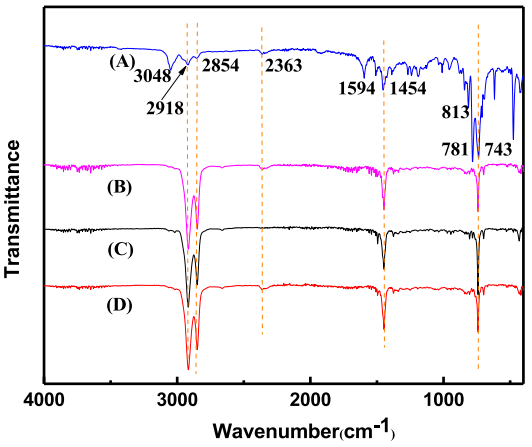

Figure 2. FT-IR spectra of WHTCT (A), products (B), DF (C), and GF (D). Reaction condition: T = 390 °C, P = 16 MPa, LHSV = 0.25 h^{-1}, and H_2/oil = 2000:1.

It can be seen from Figure 2 that the four samples have absorption peaks at 743, 1454, 2854, and 2918 cm^{-1}, which are attributed to the outer surface bending vibration peak of alkyl alcohols or phenolic OH, the in-plane bending vibration peak of C−H, the in-plane stretching vibration peak of alkyl−CH_2−, and the in-plane stretching vibration peak of alkyl C−H, respectively,[3,30] which indicate that there are hydroxyl functional groups in these four samples. For WHTCT (A), the in-plane −C═CH stretching vibration peak of olefin appears at 3048 cm^{-1}, and the in-plane bending vibration peak of the N−H appears at 1594 cm^{-1}. In addition, the outer plane bending vibration peak of olefin C−H appears in fingerprint regions at 813 and 781 cm^{-1}, indicating that there is a certain amount of unsaturated C═C bonds in WHTCT. The products (B), GF (C), and DF (D) have similar FT-IR spectra. Compared with the WHTCT spectra, there are some changes: (1) The band at 3048 cm^{-1} almost disappeared,

https://doi.org/10.1021/acsomega.2c06202
ACS Omega 2022, 7, 48163−48172

indicating that the C=C compound decreased. (2) The peaks of alkanes at 2918 and 2854 cm^{-1} became stronger, and the absorption peaks at 813 and 781 cm^{-1} almost disappeared, indicating that the content of alkanes increased while the aromatic groups decreased. (3) The band at 1594 cm^{-1} almost disappeared, indicating that the N−H bond basically does not exist. Therefore, it can be concluded that in the process of WHTCT hydrogenation, the unsaturated bond is saturated, and the covalent bonds between the heteroatom and the hydrogen atom were broken, resulting in the removal of heteroatoms.

3.2.2. GC−MS Analysis. Table 6 shows that the most abundant components in GF were C9−C12 hydrocarbons.

Table 6. Main Components of GF

molar content (%)	compound name	formula	molecular weight
1.09508	cyclohexane, ethyl-	C_8H_{16}	112
0.70739	ethylbenzene	C_8H_{10}	106
0.77705	benzene, 1,3-dimethyl-	C_8H_{10}	106
1.98756	1-ethyl-4-methylcyclohexane	C_9H_{18}	126
1.46725	cyclohexane, propyl-	C_9H_{18}	126
0.98736	1H-indene, octahydro-, trans-	C_9H_{16}	124
1.28702	benzene, 1-ethyl-3-methyl-	C9H12	120
1.9851	1H-indene, octahydro-, cis-	C_9H_{16}	124
1.68059	cyclohexane, butyl-	$C_{10}H_{20}$	140
3.95911	indane	C_9H_{10}	118
2.04235	naphthalene, decahydro-, trans-	$C_{10}H_{18}$	138
3.32917	naphthalene, decahydro-, cis-	$C_{10}H_{18}$	138
2.20358	trans-decalin, 2-methyl-	$C_{11}H_{20}$	152
2.46471	naphthalene, decahydro-2-methyl-	$C_{11}H_{20}$	152
1.76059	cis-decalin, 2-*syn*-methyl-	$C_{10}H_{20}$	140
1.16743	1H-indene, 2,3-dihydro-5-methyl-	$C_{10}H_{12}$	132
4.34058	naphthalene, 1,2,3,4-tetrahydro-	$C_{10}H_{12}$	132
0.84028	naphthalene, decahydro-2,3-dimethyl-	$C_{12}H_{22}$	166
3.28739	azulene	$C_{10}H_8$	128
2.50429	naphthalene, 1,2,3,4-tetrahydro-2-methyl-	$C_{11}H_{14}$	146
1.19463	cis,trans-3-ethylbicyclo[4.4.0]decane	$C_{12}H_{22}$	166
2.66348	acenaphthylene, dodecahydro-	$C_{12}H_{20}$	164
1.84538	tricyclo[7.3.0.0(2,6)]dodecane, trans-anti-trans-	$C_{12}H_{20}$	164
1.93481	naphthalene, 1,2,3,4-tetrahydro-6-methyl-	$C_{11}H_{14}$	146
1.61894	cyclohexane, (cyclopentylmethyl)-	$C_{12}H_{22}$	166
3.6351	1,1'-bicyclohexyl	$C_{12}H_{22}$	166
1.97906	benzene, cyclohexyl-	$C_{12}H_{16}$	160
1.20565	naphthalene, 2-ethyldecahydro-	$C_{12}H_{22}$	166
2.25543	acenaphthylene, 1,2,2a,3,4,5-hexahydro-	$C_{12}H_{14}$	158
0.72252	naphthalene, 1,2,3,4,4a,5,6,7-octahydro-4a-methyl-	$C_{11}H_{18}$	150

Also, 66.8% of cycloalkanes and 33.2% of aromatics were detected, of which tetralin had the highest content, accounting for 4.34%. Cycloalkanes were mainly bicyclic cycloalkanes (BCAs), tricyclic cycloalkanes (TCAs), and alkyl-substituted cyclohexane, which account for 40.9, 15.9, and 10%, respectively. The BCAs were mainly decahydronaphthalene, and the TCAs were mainly tetradecahydroanthracene. Alkyl-substituted cyclohexane mainly exists in the form of methyl-, propyl-, and butyl-cyclohexane, among which methyl-cyclohexane has the most content. These substituted cyclohexanes may be derived from corresponding benzene series with different branches. Aromatic compounds were dominated by monocyclic aromatics (MAs), mainly including dihydroindene, alkylbenzene, and tetrahydronaphthalene, which account for 5.4, 5.67, and 9.77%, respectively. Compared with the composition of GF derived from LTCT, the GF does not contain olefins and paraffins but have relatively higher proportion of BCAs; this is attributed to the high content of naphthalene in WHTCT, which can be converted into trans- and cis-decalin by hydrogenation.[32] Due to the poor thermodynamic stability of cis-decalin, it can be easily converted to trans-decalin. Therefore, the content of trans-decalin in gasoline is significantly higher than that of cis-decalin.[33] Another observation is that the GF contains a large amount of BCAs and TCAs.

The distribution of the compounds in the DF is listed in Table 7, mainly including cycloalkanes, MA, and a small amount of four-ring structure compounds. Among them, cycloalkanes have the dominant proportion and contain significant amounts of alkyl cyclohexane, alkyl decahydronaphthalene, tetradecahydroanthracene, and hexahydropyrene. BCAs and TCAs account for 25.1 and 26.3%, respectively. Tricyclododecane and tetradecahydroanthracene account for a relatively high proportion of TCA, indicating that the DF is rich in BCAs and TCAs. MAs include alkyl-substituted benzene (AB), tetrahydronaphthalene (AT), hexahydrofluorene (HF), and octahydroanthracene (OA), of which AT was the dominant component, which accounted for about 11.1%. The relative distribution of aromatics decreases as the number of rings increases, mainly because the hydrogenation of the last ring of polycyclic aromatics was much more difficult than those of the first two rings.[34,35] Therefore, 28.4% MA still existed in the DF.

Table 7. Hydrocarbon Distribution of DF

hydrocarbon types	hydrocarbon distribution (wt %)
MCA	4.4
BCA	25.1
TCA	26.3
TECA	11.1
total cycloalkanes	66.9
AB	5.4
indanes	2.7
indenes	1.2
AT and HF	14.2
OA and OP	4.9
total MA	28.4
total DA	4.7
total aromatics	33.1
total	100

3.3. Properties of GF and DF. Table 8 lists the physical and chemical properties of GF and DF. Compared with the China V vehicle gasoline standard, it was found that the GF has a higher density value and a lower octane number (RON), and other main performances such as the distillation range, S content, and gum content meet the requirements of gasoline specifications. This indicated that the GF could not be used directly as motor fuel but could be used as a gasoline blending component or solvent oil.

https://doi.org/10.1021/acsomega.2c06202
ACS Omega 2022, 7, 48163−48172

Table 8. Physical and Chemical Properties of GF and DF

	GF		DF	
properties	specification requirements GB17930-2016[a]	tested value	specification requirements GB 19147-2016[b]	tested values
distillation range (°C)				
10%	≤70	65		
50%	≤120	120	≤300	275
90%	≤190	175	≤355	322
95%			≤365	345
FBP	≤205	202		362
density (20 °C) (g mL^{-1})	0.720∼0.775	0.805	0.79∼0.85	0.912
sulfur (wt %)	0.001	0.00062	0.001	0.00085
nitrogen (wt %)		0.0012		0.0035
corrosion with Cu (50 °C, 3 h)	≤1	0.5	≤1	0.5
existent gum (mg·100 mL^{-1})	≤5	3.5	≤5	2.5
acid value (KOH) (mg mL^{-1})			≤7	5.0
induction period (min)	≥480	492		
aromatics (wt %)	≤40			
PAHS (wt %)			≤11	4.7
solidifying point (°C)				−36
RON	≥92	85		
cetane number			≥47	43

[a]Gasoline for motor vehicles (China V). [b]Automobile diesel fuels (China V).

In the DF, polycyclic aromatic hydrocarbon compounds (PAHS) accounted for only 4.7%, and the S and N contents are very low, respectively, 8.5 and 35 μg/g, with a lower freezing point, relatively small cetane number (CN 43), and higher density; it could be used as a blending component of high-quality low-freezing point diesel. Second, these components contained a large amount of decalin, which could effectively improve the high-temperature degradation ability and could be used as a JP-900 jet fuel-based oil.[36]

3.4. Component Conversion Kinetics. Establishing a component kinetic model was an convenient method to study the conversion between each component, and it can also be used to enhance the yield of light fractions in the hydrogenation process. The preceding studies have shown that temperature and LHSV have a significant impact on the reaction process. Therefore, the hydrogenation test was carried out upon the following typical conditions: temperature (375, 390, and 405 °C), LHSV (0.25, 0.3, and 0.35 h^{-1}), pressure (16 MPa), and the H_2/oil ratio (2000:1), establishing a lumped kinetic model to study the transformation law of each component in WHTCT.

3.4.1. Component Division. In the lumped kinetic model, the feedstock and product are divided into the following four lumps based on their distillation range: Lumped 1-TO (>360 °C); Lumped 2-DF (180∼360 °C); Lumped 3-GF (IBP ∼ 180 °C); and Lumped 4-gas.

3.4.2. Kinetic Model. The Lumped kinetic model and reaction network are shown in Figure 3. The kinetic model included four lumped (TO, DF, GF, and gas) and nine kinetic parameters (k_{12}, k_{13}, k_{14}, k_{23}, k_{24}, k_{34}, n_1, n_2, and n_3). The product composition was estimated by the mass balance during the test, and the reaction rate expression is shown in eq 1.

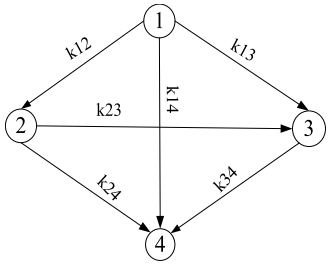

Figure 3. 4 Lumped kinetic model and reaction network.

$$\begin{cases} r_1 = -(k_{12} + k_{13} + k_{14})y_1^{n_1} \\ r_2 = k_{12}y_1^{n_1} - (k_{23} + k_{24})y_2^{n_2} \\ r_3 = k_{13}y_1^{n_1} + k_{23}y_2^{n_2} - k_{34}y_3^{n_3} \\ r_4 = k_{14}y_1^{n_1} + k_{24}y_2^{n_2} + k_{34}y_3^{n_3} \end{cases} \quad (1)$$

The kinetic model was included in a isothermal reactor model,[16−18,20] which was established by using the following assumptions:

(a) The reactor operates in isothermal mode.
(b) There is no radial concentration gradient in the reactor.
(c) The reactor is operated in the steady state.
(d) The model is a one-dimensional steady-state model.
(e) The phase transition of light components is negligible.

The following mass balance equation eq 2 was used to estimate the composition of the product:

$$\frac{dy_i}{dt} = \frac{dy_i}{d(1/\mathrm{LHSV})} = r_i \quad (2)$$

The reaction rate constants in the kinetic model can be calculated using eq 3.[16]

$$k = k_0 \exp(-E_a/RT) \quad (3)$$

https://doi.org/10.1021/acsomega.2c06202
ACS Omega 2022, 7, 48163−48172

Table 9. Experimental and Predicted Product Compositions

LHSV/h^{-1}		0	0.25			0.3			0.35		
T	lumps	feed/wt %	EV/wt %	PV/wt %	RE/%	EV/wt %	PV/wt %	RE/%	EV/wt %	PV/wt %	RE/%
375	gas	0.35	0.82	0.79	−3.66	1.31	1.36	3.82	1.04	1.09	4.81
	GF	9.15	14.14	13.98	−1.13	13.69	13.26	−3.14	11.52	12.04	4.51
	DF	56.97	73.62	71.64	−2.69	72.48	70.75	−2.39	72.01	71.21	−1.11
	TO	33.53	11.42	10.88	−4.73	12.52	11.94	−4.63	15.43	14.73	−4.54
390	gas	0.35	0.95	0.91	−4.21	0.73	0.71	−2.74	0.54	0.52	−3.70
	GF	9.15	16.71	15.94	−4.61	14.69	15.02	2.25	12.43	13.05	4.99
	DF	56.97	74.89	74.36	−0.71	74.35	73.54	−1.09	71.81	72.94	1.57
	TO	33.53	7.45	7.245	−2.75	10.23	9.82	−4.01	15.22	14.64	−3.81
405	gas	0.35	1.84	1.76	−4.35	0.92	0.89	−3.26	0.63	0.65	3.17
	GF	9.15	21.56	21.94	1.76	15.74	15.94	1.27	14.34	15.04	4.88
	DF	56.97	73.46	71.84	2.21	75.22	73.84	−1.83	73.15	73.43	0.38
	TO	33.53	3.14	3.21	2.23	8.12	8.32	2.46	11.88	11.36	−4.38

where y_i, component mass fraction, %; k, apparent reaction rate constant; t, reactant residence time, h; k_0, exponential factor; E_a, apparent activation energy, J mol^{-1}.

In order to obtain the best values of the kinetic parameters of all experiments, the sum of squares errors between the experimental values (y_i^{exp}) and the calculated values (y_i^{cal}) was minimized using the optimization technique by eq 4.[37]

$$SSE = \sum_{i=1}^{m} [y_i^{exp} - y_i^{cal}]^2 \quad (4)$$

3.4.3. Model and Kinetic Parameters. The experimental and the predicted composition values of the model are listed in Table 9.

Table 9 shows that as the temperature increases and the LHSV decreases, the TO yield decreases, causing the yield of GF and DF to increase, which indicated that the high boiling point macromolecules in the TO converted to small molecule compounds through hydrogenation, further showing that the conversion of TO to DF and GF occurs. The yields of GF and DF reached the highest points of 21.56 and 73.46% at 405 °C and 0.25 h^{-1}, which shows that the TO can obtain the highest conversion under this condition. The comparison between the predicted data and the experimental value is shown in Figure 4, which illustrated that the R_2 of the linear fitting curve value is 0.9996, and the slope of the straight line is almost 1, indicating that the predicted data show well agreement with the experimental value and the model have high reliability prediction.

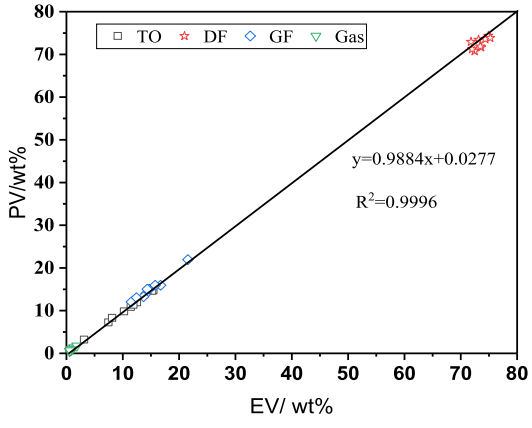

Figure 4. Comparison of predicted and experimental values.

The estimated model kinetic parameters are shown in Table 10. In the range of operating conditions, the value of the reaction rate constant k_{34} is almost close to 0, which indicated that the GF will hardly be converted to gas. Although the reaction rate constant k_{24} was larger than k_{34}, these values were still small, indicating that DF is difficult to convert to gas even at higher temperatures. Therefore, gas can only be obtained through TO conversion. It can be judged by the reaction rate constants k_{12}, k_{13}, and k_{14} that the TO can be converted into DF and GF with high selectivity. At 375 °C, the reaction rate constant k_{23} is very small, while the temperature is higher than 390 °C, k_{23} increases significantly, indicating that DF is rarely converted to GF at lower temperatures, and the conversion of DF to gas was accelerated over 390 °C. It can also be found from Table 10 that as the temperature increases, all the reaction rate constants show an increasing trend, which further shows that the increase in temperature is conducive to improving the reactivity of the components and promoting the conversion of heavy components to light components.

4. CONCLUSIONS

In this study, the effect of operating severity on the quality of the products obtained during hydrotreating of WHTCT in a pilot-scale TBR filled with an industrial NiMo/SiO_2-Al_2O_3 catalyst was investigated. The results indicated that the FBP, the density, and the sulfur and nitrogen content of the products decrease, the H/C ratio increases with the elevated temperature and pressure and the declined LHSV, resulting in the improvement of the oil quality, and the S and N concentrations in the feedstocks decreased from 4600 and 6800 μg/g to 24.06 and 14.32 μg/g, respectively, in the products under a temperature of 390 °C, pressure of 16 MPa, and LHSV of 0.25 h^{-1}, illustrating that WHTCT can be utilized as a suitable feedstock to obtain clean fuel oil through hydrogenation.

The chemical composition of the product was analyzed by FT-IR and GC−MS. Compared with the China V gasoline and diesel standard, the GF has a higher density and a lower RON, and all other main performances meet the requirements for it to be used as a clean gasoline blending component or solvent oil. The content of PAHS (4.7%) in the DF is far below the requirement of the standards (11%). Except for the higher density and lower CN, other indexes can meet the requirements; in particular, the DF has a lower freezing point.

https://doi.org/10.1021/acsomega.2c06202
ACS Omega 2022, 7, 48163−48172

Table 10. Estimated Kinetic Parameters

reaction order	reaction rate constant	temperature/°C			E_a/kJ/mol
		375	390	405	
n_1 = 1.532		TO			
	k_{12}	0.00452	0.0235	0.0613	125.3
	k_{13}	0.00032	0.0124	0.0278	71.45
	k_{14}	0.00022	0.00652	0.0125	100.2
n_2 = 1.214		DF			
	k_{23}	0.00014	0.00566	0.00654	143.6
	k_{24}	0.00005	0.00013	0.00026	86.9
n_3 = 1.012		gas			
	k_{34}	0.0000012	0.0000041	0.0000068	13.24

In the range of operating conditions, the TO can be converted into DF and GF with high reaction selectivity. DF is difficult to be converted to GF at a lower temperature, and the GF hardly undergoes cracking reaction to procuce gas. The lumped kinetic model can accurately predict the weight fraction of TO, DF, GF, and gas under different hydrogenation conditions with average relative error less than 5%.

After deep hydro-upgrading of WHTCT, the products are rich in BCAs and TCAs, resulting in high density, low RON, and CN for GF and DF, and cannot be directly used as vehicle fuel oil. However, it has potential in preparation of high-density jet fuel. In the future research, the hydrogenation process can be optimized to produce high value-added military or aerospace fuels.

AUTHOR INFORMATION

Corresponding Author

Xiaoyong Fan − *School of Chemistry and Chemical Engineering, Shaanxi Key Laboratory of Low Metamorphic Coal Clean Utilization, Yulin University, Yulin 719000, People's Republic of China; School of Chemical Engineering, Northwest University, Xi'an 710069, People's Republic of China;* orcid.org/0000-0002-6351-1778; Phone: +86-15929199059; Email: fanxy@yulinu.edu.cn

Authors

Dong Li − *School of Chemical Engineering, Northwest University, Xi'an 710069, People's Republic of China;* orcid.org/0000-0002-4578-0595

Louwei Cui − *The Northwest Research Institute of Chemical Industry, Xi'an 710069, People's Republic of China*

Chunran Chang − *School of Chemistry and Chemical Engineering, Shaanxi Key Laboratory of Low Metamorphic Coal Clean Utilization, Yulin University, Yulin 719000, People's Republic of China; Shaanxi Key Laboratory of Energy Chemical Process Intensification, School of Chemical Engineering and Technology, Xi'an Jiaotong University, Xi'an 710049, People's Republic of China*

Long Yan − *School of Chemistry and Chemical Engineering, Shaanxi Key Laboratory of Low Metamorphic Coal Clean Utilization, Yulin University, Yulin 719000, People's Republic of China*

Bo Yang − *School of Chemistry and Chemical Engineering, Shaanxi Key Laboratory of Low Metamorphic Coal Clean Utilization, Yulin University, Yulin 719000, People's Republic of China*

Complete contact information is available at: https://pubs.acs.org/10.1021/acsomega.2c06202

Notes

The authors declare no competing financial interest.

ACKNOWLEDGMENTS

The financial support of this work is provided by the Dr. Scientific Research Fund of Yulin university (22GK05), Youth Innovation Team Research Program Project of Shaanxi Provincial Department of Education (22JP104), the innovation Capability Support Program of Shaanxi (2020TD-028), the Technology Innovation Leading Program of Shaanxi (2019CGHJ-11), and the Science and Technology Plan of Yulin Government (CXY-2020-002-07).

REFERENCES

(1) Yue, Y.; Li, J.; Dong, P.; Wang, T.; Jiang, L.; Yuan, P.; Zhu, H.; Bai, Z.; Bao, X. From cheap natural bauxite to high-efficient slurry-phase hydrocracking catalyst for high temperature coal tar: A simple hydrothermal modification. *Fuel Process. Technol.* **2018**, *175*, 123−130.

(2) Xie, K.; Li, W. Y.; Zhao, W. Coal chemical industry and its sustainable development in China. *Energy* **2010**, *35*, 4349−4355.

(3) Kan, T.; Wang, H.; He, H.; Li, C.; Zhang, S. Experimental study on two-stage catalytic hydroprocessing of middle-temperature coal tar to clean liquid fuels. *Fuel* **2011**, *90*, 3404−3409.

(4) Li, D.; Cui, W.; Zhang, X.; Meng, Q.; Zhou, Q.; Ma, B.; Niu, M.; Li, W. Production of Clean Fuels by Catalytic Hydrotreating a Low Temperature Coal Tar Distillate in a Pilot-Scale Reactor. *Energy Fuels* **2017**, *31*, 11495−11508.

(5) Gu, Z.; Chang, N.; Hou, X.; Wang, J.; Liu, Z. Experimental study on the coal tar hydrocracking process in supercritical solvents. *Fuel* **2012**, *91*, 33−39.

(6) Ma, Z. H.; Wei, X. Y.; Liu, G. H.; Liu, F. J.; Zong, Z. M. Value-added utilization of high-temperature coal tar: A review. *Fuel* **2021**, *292*, No. 119954.

(7) Han, L.; Zhang, R.; Bi, J. Experimental investigation of high-temperature coal tar upgrading in supercritical water. *Fuel Process. Technol.* **2009**, *90*, 292−300.

(8) Chang, N.; Gu, Z.; Wang, Z.; Liu, Z.; Hou, X.; Wang, J. Study of Y zeolite catalysts for coal tar hydro-cracking in supercritical gasoline. *J. Porous Mater.* **2011**, *18*, 589−596.

(9) Bellussi, G.; Rispoli, G.; Landoni, A.; Millini, R.; Molinari, D.; Montanari, E.; Moscotti, D.; Pollesel, P. Hydroconversion of heavy residues in slurry reactors: Developments and perspectives. *J. Catal.* **2013**, *308*, 189−200.

(10) Angeles, M.; Leyva, C.; Ancheyta, J.; Ramirez, S. A Review of Experimental Procedures for Heavy Oil Hydrocracking with Dispersed Catalyst. *Catal. Today* **2014**, *220*, 274−294.

(11) Majka, M.; Tomaszewicz, G.; Mianowski, A. Experimental study on the coal tar hydrocracking process over different catalysts. *J. Energy Inst.* **2018**, *91*, 1164−1176.

(12) Ancheyta, J.; Betancourt, G.; Marroquín, G.; Castañeda, L. C.; Alonso, F.; Muñoz, J. A.; Gómez, M. T.; Rayo, P. Hydroprocessing of

Maya heavy crude oil in two reaction stages. *Appl. Catal. A: Gen.* **2002**, *233*, 159−170.
(13) Zhao, G. F.; Yao, C. L.; Quan, H. The Research of Anthracene Oil Hydro-upgrading. *Contemp. Chem. Ind.* **2008**, *37*, 341−343.
(14) Yan, J.; Lv, C. S.; Liu, A. H. Production of Gasoline and Diesel Oil by Hydrogenation of High Temperature Coal Tar. *Petrochem. Technol.* **2006**, *35*, 33−36.
(15) Jarullah, A. T.; Mujtaba, I. M.; Wood, A. S. Enhancement of Productivity of Distillate Fractions by Crude Oil Hydrotreatment: Development of Kinetic Model for the Hydrotreating Process. *Comput. Aided Chem. Eng.* **2011**, 261−265.
(16) Feng, X.; Shen, Z.; Li, D.; Liu, X.; Fan, X.; Zheng, H.; Dan, Y.; Li, W. Kinetic parameter estimation and simulation of trickle-bed reactor for hydrodenitrogenation of whole-fraction low-temperature coal tar. *Energy Sources A: Recovery Util. Environ. Eff.* **2019**, *41*, 802−810.
(17) Feng, X.; Li, D.; Chen, J.; Niu, M.; Liu, X.; Lester, C.; Li, W. Kinetic Parameter Estimation and Simulation of Trickle-Bed Reactor for Hydrodesulfurization of Whole Fraction Low Temperature Coal Tar. *Fuel* **2018**, *230*, 113−125.
(18) Liu, X.; Li, D.; Feng, X.; Zheng, H.; Lu, L.; Fan, X.; Li, W. Kinetics study and reactor simulation of full-range low-temperature coal tar during hydrodeoxygenation process. *Energy Sources A: Recovery Util. Environ. Eff.* **2019**, *41*, 2725−2733.
(19) Speight, J. G., *The Desulfurizaiton of Heavy Oils and Residua*; Marcel Dekker: New York2000.
(20) Fan, X.; Li, D.; Dan, Y.; Dong, H.; Guo, Q.; Zheng, H.; Li, W. Kinetic Parameter Calculation and Trickle Bed Reactor Simulation Based on Pilot-Scale Hydrodesulfurization Test of High-Temperature Coal Tar. *ACS Omega* **2020**, *5*, 12923−12936.
(21) Wang, R.; Ci, D.; Cui, X.; Bai, Y.; Liu, C.; Kong, D.; Zhao, S.; Long, Y.; Guo, X. Pilot-plant study of upgrading of medium and low-temperature coal tar to clean liquid fuels. *Fuel Process. Technol.* **2017**, *155*, 153−159.
(22) Velegol, D.; Gautam, M.; Shamsi, A. Catalytic cracking of a coal tar in a fluid bed reactor. *Powder Technol.* **1997**, *93*, 93−100.
(23) Ancheyta-Juárez, J.; Betancourt-Rivera, G.; Marroquín-Sánchez, G.; Pérez-Arellano, A. M.; Maity, S. K.; Cortez, M. T.; del Río-Soto, R. An Exploratory Study for Obtaining Synthetic Crudes from Heavy Crude Oils via Hydrotreating. *Energy Fuels* **2000**, *15*, 120−127.
(24) Gioia, F.; Ee, L. V. Effect of hydrogen pressure on catalytic hydrodenitrogenation of quinoline. *Ind. Eng. Chem. Process Des. Dev.* **1986**, *25*, 918−925.
(25) Leckel, D. Catalytic Hydroprocessing of Coal-Derived Gasification Residues to Fuel Blending Stocks: Effect of Reaction Variables and Catalyst on Hydrodeoxygenation (HDO), Hydrodenitrogenation (HDN), and Hydrodesulfurization (HDS). *Energy Fuels* **2006**, *20*, 1761−1766.
(26) Topsoe, C. H. Catalyst and Process Technologies for Ultra Low Sulfur Diesel. *Appl. Catal., A: Gen.* **1999**, *189*, 205−215.
(27) Li, D.; Li, Z.; Li, W.; Liu, Q.; Feng, Z.; Fan, Z. Hydrotreating of Low Temperature Coal Tar to Produce Clean Liquid Fuels. *J. Anal. Appl. Pyrolysis* **2013**, *100*, 245−252.
(28) Wei, Q.; Wen, S.; Tao, X.; Zhang, T.; Zhou, Y.; Chung, K.; Xu, C. Hydrodenitrogenation of Basic and Non-Basic Nitrogen-Containing Compounds in Coker Gas Oil. *Fuel Process. Technol.* **2015**, *129*, 76−84.
(29) Sun, R.; Shen, S.; Zhang, D.; Ren, Y.; Fan, J. Hydrofining of Coal Tar Light Oil to Produce High Octane Gasoline Blending Components over Gamma-Al_2O_3- and Eta-Al_2O_3-Supported Catalysts. *Energy Fuels* **2015**, *29*, 7005−7013.
(30) Cui, W.; Li, W.; Rong, G.; Ma, H. Hydroprocessing of Low-Temperature Coal Tar for the Production of Clean Fuel over Fluorinated NiW/Al_2O_3-SiO_2 Catalyst. *Energy Fuels* **2017**, *31*, 3768−3783.
(31) Miranda, R.*Mechanism of hydrodenitrogenation H(sub 2)-D(sub 2) exchange in non-acidic and acidic supports*. 1991, *30*, 1 −13.
(32) Liu, Y. C.*Study on Selective Catalytic Hydrogenation of Polycyclic Aromatic Hydrocarbons*; Dalian University of Technology, 2013.
(33) Korre, S. C.; Klein, M. T.; Quann, R. J. Polynuclear Aromatic Hydrocarbons Hydrogenation. 1: Experimental Reaction Pathways and Kinetics. *Ind. Eng. Chem. Res.* **1995**, *34*, 101−117.
(34) Stanislaus, A.; Cooper, B. H. Aromatic Hydrogenation Catalysis: A Review. *Catalysis Reviews* **1994**, *36*, 75−123.
(35) Chareonpanich, M.; Zhang, Z. G.; Tomita, A. Hydrocracking of Aromatic Hydrocarbons over USY-Zeolite. *Energy Fuels* **1996**, *10*, 927−931.
(36) Berkhous, S. K.*Thermal Oxidative Stability of Coal-Based JP-900 Jet Fuel: Impact on Selected Physical Properties*; The Pennsylvania State University, 2007.
(37) Fan, X. Y.; Li, D.; Feng, X.; Dong, H.; Liu, X.; Dan, Y.; Zheng, H.; Fan, A.; Li, W. Modelling and simulation of industrial trickle bed reactor hydrotreating for whole fraction low-temperature coal tar simultaneous hydrodesulfurisation and hydrodenitrification. *Fuel* **2020**, *269*, No. 117362.

https://doi.org/10.1021/acsomega.2c06202
ACS Omega 2022, 7, 48163−48172